Appendices

A.1. Analysis of Remanent Flux in Proposed Integrated Magnetic Structure

In order to find the worst-case maximum flux density in each core leg, one must find the worst-case remanent flux density distribution in each core leg. If the direction of the remanent flux density of each core leg is the same as that defined in Figure A-1, the remanent flux density will add up the dc flux density and the ac flux density, and the worst-case maximum density can be obtained.

To calculate the worst-case remanent flux density, it is necessary to identify the remanent flux density and magnetic field intensity inside each core leg. outer leg 1 is used as the example to illustrate (see Figure A-2). As shown in Figure A-3, the remanent flux density, B_{1r}, after the gapping is smaller than the original remanence, B_r, when the core is not gapped. If there is a remanent flux, j_{1r}, or the flux density B_{1r} in the core portion A_1, the remanent flux density in the air gap l_{1g} should be the same assuming that no flux fringing exists. Based on Figure A-3, we have

$$H_{1g} = \frac{B_{1g}}{m_0} = \frac{B_{1r}}{m_0} \qquad \textbf{Eq. A-1}$$

$$H_{1c} = \frac{B_{1r} - B_r}{m_0 m_r} \qquad \textbf{Eq. A-2}$$

where m_r and B_r are the relative permeability and the remanent flux density, respectvely, for the selected ferrite material (ungapped).

Because of the flux continuity in outer leg 1, the magnetizing force or the magnetic field strength in the base plate or bottom of the E-core (l_{1cb}, A_{1b} portion in Figure A-2) can be estimated to be

$$H_{1cB} = \frac{B_{1br} - B_r}{m_0 m_r} = \frac{B_{1r}\dfrac{A_1}{A_{1b}} - B_r}{m_0 m_r} \qquad \textbf{Eq. A-3}$$

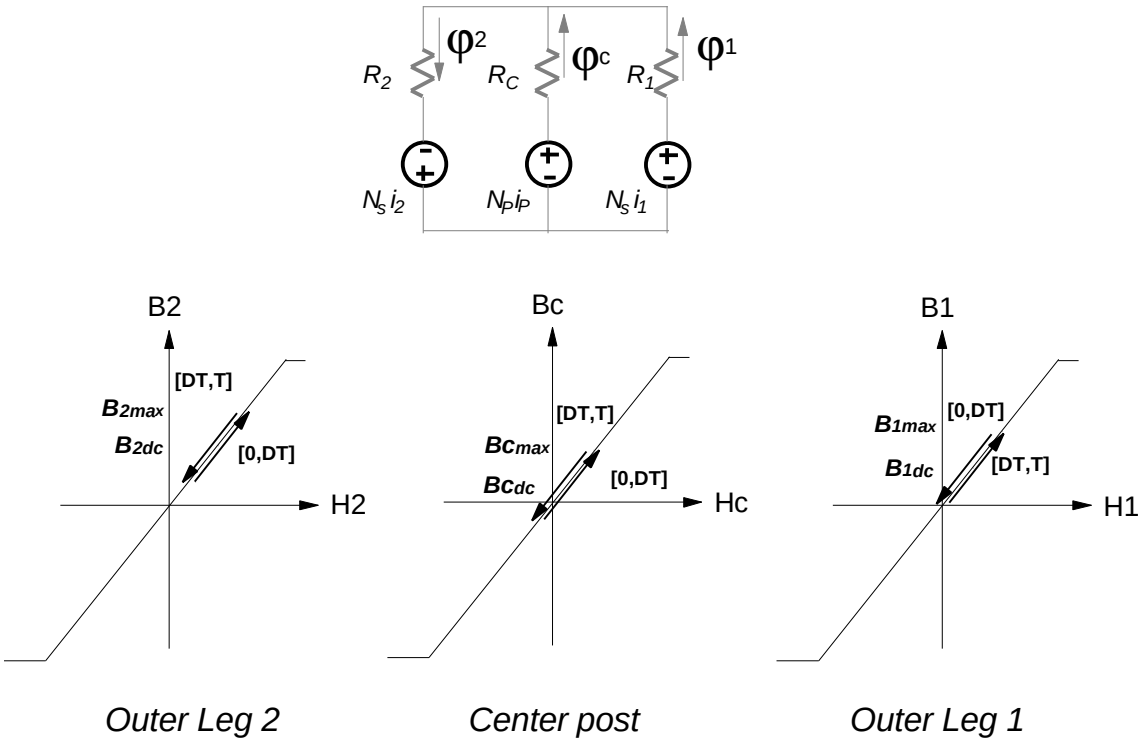

Figure A-1 Flux distribution within each core leg

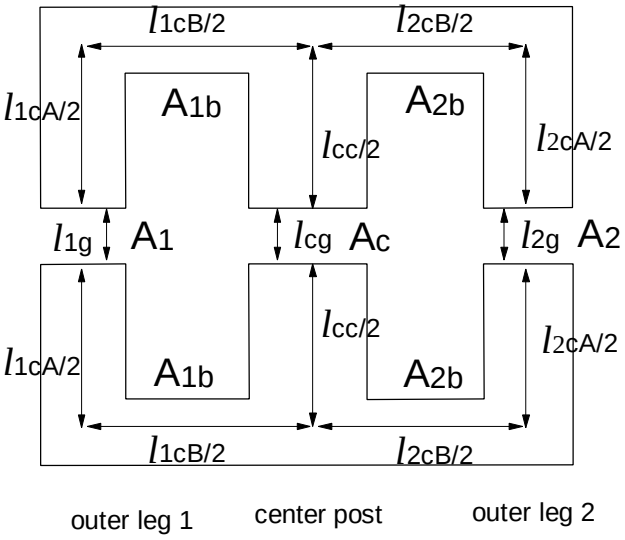

Figure A-2 Dimensions of integrated magnetic core

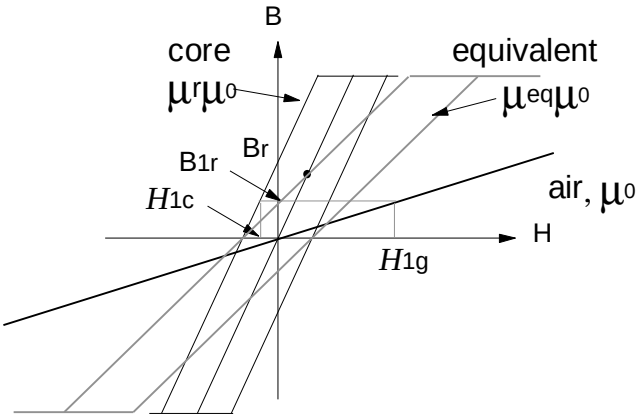

Figure A-3 Sketch of remanent flux in outer leg 1

Following a similar procedure, we can derive the magnetizing forces or the magnetic field strengths for the center post and outer leg 2:

Outer leg 2:

$$H_{2g} = \frac{B_{2r}}{m_0} \qquad \textbf{Eq. A-4}$$

$$H_{2c} = \frac{B_{2r} - B_r}{m_0 m_r} \qquad \textbf{Eq. A-5}$$

$$H_{2cB} = \frac{B_{2r}\dfrac{A_2}{A_{2b}} - B_r}{m_0 m_r} \qquad \textbf{Eq. A-6}$$

Center post:

$$H_{cg} = \frac{B_{cr}}{m_0} \qquad \textbf{Eq. A-7}$$

$$H_{cc} = \frac{B_{cr} - B_r}{m_0 m_r} \qquad \textbf{Eq. A-8}$$

If we apply Ampere's Law to the loop consisting of outer leg 1 and outer leg 2, and the loop consisting of outer leg 1 and center post, we can obtain the following equations:

$$H_{1g}l_{1g} + H_{1c}l_{1cA} + H_{1cB}l_{1cB} + H_{2g}l_{2g} + H_{2c}l_{2cA} + H_{2cB}l_{2cB} = N_1 i_1 + N_2 i_2 = 0 \qquad \textbf{Eq. A-9}$$

$$H_{1g}l_{1g} + H_{1c}l_{1cA} + H_{1cB}l_{1cB} - H_{cg}l_{cg} - H_{cc}l_{cc} = N_1 i_1 - N_p i_p = 0 \qquad \textbf{Eq. A-10}$$

The definition of the dimensions can be found in Figure A-2.

By substituting Eqs. A-1 through A-8 into Eqs. A-9 and A-10, we can get

$$B_{1r}\left(l_{1g} + \frac{l_{1cA} + l_{1cB}\dfrac{A_1}{A_{1B}}}{m_r}\right) + B_{2r}\left(l_{2g} + \frac{l_{2cA} + l_{2cB}\dfrac{A_2}{A_{2B}}}{m_r}\right) = B_r\left(\frac{l_{1cA} + l_{1cB} + l_{2cA} + l_{2cB}}{m_r}\right)$$

Eq. A-11

$$B_{1r}\left(l_{1g} + \frac{l_{1cA} + l_{1cB}\dfrac{A_1}{A_{1B}}}{m_r}\right) - B_{cr}\left(l_{gc} + \frac{l_{cc}}{m_r}\right) = B_r\left(\frac{l_{1cA} + l_{1cB} - l_{cc}}{m_r}\right) \qquad \textbf{Eq. A-12}$$

The relationship among the fluxes of the three core legs gives

$$B_{1r}A_1 + B_{cr}A_c = B_{2r}A_2. \qquad \textbf{Eq. A-13}$$

By solving Eqs. A-11 through A-13, we have

$$B_{1r} = \frac{\dfrac{C_1}{K_2}A_2 + \dfrac{C_2}{K_c}A_c}{A_1 + \dfrac{K_1}{K_c}A_c + \dfrac{K_1}{K_2}A_2}B_r \qquad \textbf{Eq. A-14}$$

$$B_{2r} = \frac{\dfrac{C_1}{K_2}A_1 + \dfrac{C_1 - C_2}{K_c}A_c\dfrac{K_1}{K_2}}{A_1 + \dfrac{K_1}{K_c}A_c + \dfrac{K_1}{K_2}A_2}B_r \qquad \textbf{Eq. A-15}$$

$$B_{cr} = \frac{\dfrac{K_1}{K_2K_c}A_2(C_1 - C_2) - \dfrac{C_2}{K_c}A_1}{A_1 + \dfrac{K_1}{K_c}A_c + \dfrac{K_1}{K_2}A_2}B_r \qquad \textbf{Eq. A-16}$$

where

$$K_1 = l_{1g} + \frac{l_{1cA} + l_{1cB}\dfrac{A_1}{A_{1B}}}{m_r}$$

$$K_2 = l_{2g} + \frac{l_{2cA} + l_{2cB}\dfrac{A_2}{A_{2B}}}{m_r}$$

$$K_c = l_{cg} + \frac{l_{cc}}{m_r} \qquad \textbf{Eq. A-17}$$

$$C_1 = \frac{l_{1cA} + l_{1cB} + l_{2cA} + l_{2cB}}{m_r}$$

$$C_2 = \frac{l_{1cA} + l_{1cB} - l_{cc}}{m_r}$$

Example: E32/6.4/20 (Philips Planar Magnetics) E-E combination

- Core lengths: l_{1cA}= l_{2cA}=9.6mm, l_{1cB}= l_{2cB}=28.6mm, l_{cc}=9.6mm
- Core cross-sectional areas: A_1=A_2=70mm^2, A_{1B}=A_{2B}=65mm^2, A_c=130mm^2
- 3F3 materials: 100^{0}C core temperature, μ_r=2800, B_r=150mT
- Gap lengths: l_{1g}= l_{2g}=0.18mm, l_{cc}=0
- Based on Eqs. A-14 through A-17, the remanent fluxes are estimated as:

  outer leg 1: B_{1r}=8mT

  outer leg 2: B_{2r}=13mT

  Center Post: Bc_r=3mT

- If the air gap length is 1% of the core leg magnetic mean length, the remanence is only 5% of the ungapped value
- If the outer legs are properly gapped, the center post gapping does not have much influence on the overall remanences.

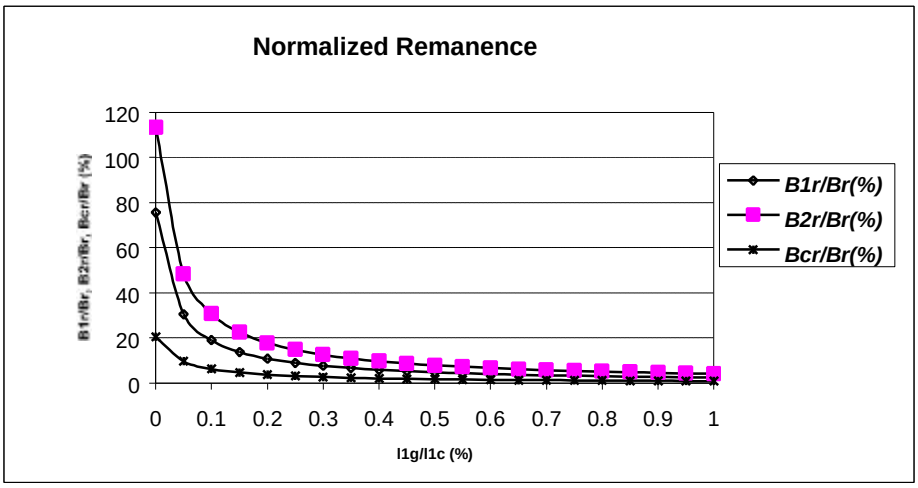

Figure A-4 Influence of outer leg gaps on the remanent fluxes

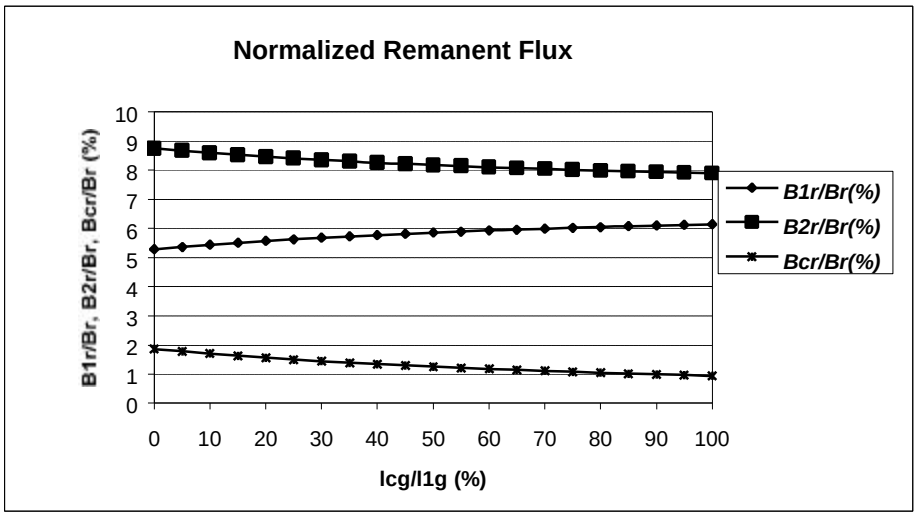

Figure A-5 Influence of center post gap on the remanent fluxes

A.2. Derivation of Small Signal Model for Forward Improved IM Circuit

Figure A-6 shows the electrical equivalent circuit for small signal analysis. The parasitic elements, including the leakage inductance, the junction capacitances of the MOSFETs, the ESR and ESL of the capacitor, and the resistance in the conduction path (including traces, windings, and semiconductor devices), are neglected in this analysis. In Figure A-6(b), all of the secondary side components are reflected to the primary side. The relationships between the reflected components and the original ones are given as follows:

$$\begin{aligned} L_{1p} &= L_1 N^2 \\ L_{2p} &= L_2 N^2 \\ C_{fp} &= C_f \big/ N^2 \\ R_{Lp} &= R_L N^2 \\ I_{op} &= \frac{I_o}{N} \\ V_{op} &= N V_o \end{aligned} \qquad \textbf{Eq. A-18}$$

where N is the primary-to-secondary turns ratio.

There are three inductors and two capacitors. The power stage appears to be a fifth-order system. The inductor currents: i_{L1p}, i_{L2p}, and i_m and the capacitor voltages: V_c and V_{op} are the variables for the state space equations. However, a close examination of the three inductors reveals that only two of the three inductor currents will be independent variables.

The fluxes in the three core legs are related as

$$j_c = j_2 - j_1 \qquad \textbf{Eq. A-19}$$

Recalling one definition of the inductance,

$$L = \frac{j}{I} \qquad \textbf{Eq. A-20}$$

produces the following equation

$$L_m i_m = L_{2p} i_{2p} - L_{1p} i_{1p}\,. \qquad \textbf{Eq. A-21}$$

It becomes obvious that only two inductor currents are independent variables. In order to facilitate the stability analysis, the current of L_m can be expressed as the function of the other two inductor currents:

$$i_m = \frac{L_{2p}}{L_m} i_{2p} - \frac{L_{1p}}{L_m} i_{1p} \qquad \textbf{Eq. A-22}$$

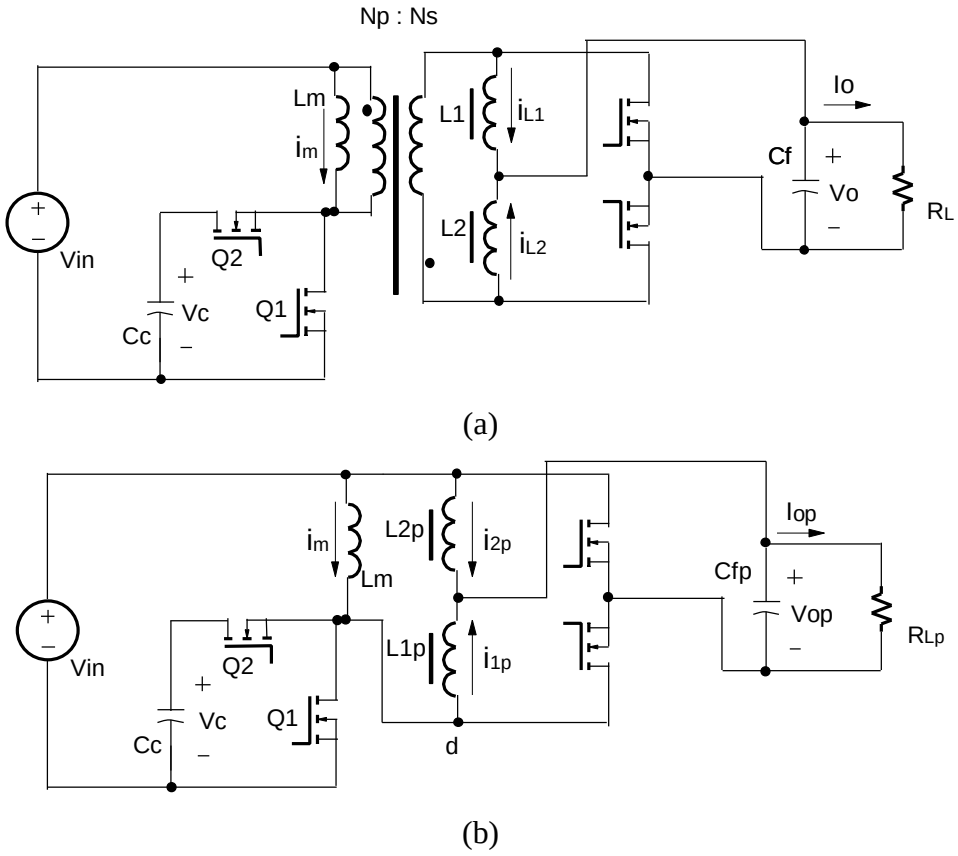

Figure A-6 Equivalent electrical circuit of FI^{2}M: (a) original, (b) reflected to the primary side

A.2.1. State Space Average Model

Figure A-7 shows the two operation stages for the steady state. For [0, DT], the following equations can be derived:

$$
\begin{aligned}
L_m \frac{di_m}{dt} &= v_{in} \\
L_{1p} \frac{di_{1p}}{dt} &= -v_{op} \\
L_{2p} \frac{di_{2p}}{dt} &= v_{in} - v_{op} \\
C_c \frac{dv_c}{dt} &= 0 \\
C_{fp} \frac{dv_{op}}{dt} &= i_{1p} + i_{2p} - \frac{v_{op}}{R_{LP}}
\end{aligned}
\qquad \textbf{Eq. A-23}
$$

The first three equations in Eq. A-23 are linearly related (3^{rd}-2^{nd}=1^{st}), as we predicted. Thus, only two inductor currents are used as the independent variables in deriving of the average state space model.

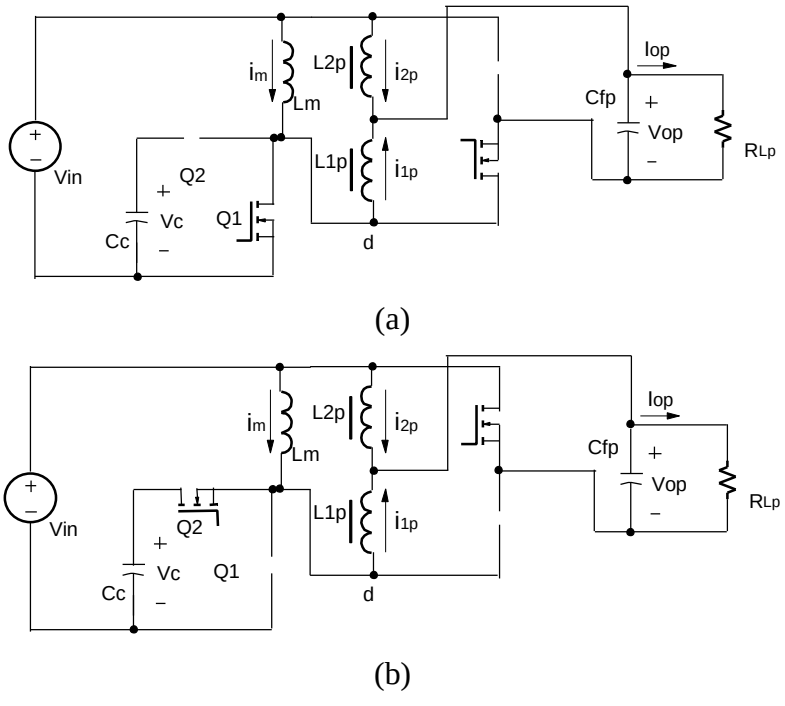

Figure A-7 Two stages for steady state operations

If we define the state variable as

$$x = \begin{bmatrix} i_{1p} & i_{2p} & v_c & v_{op} \end{bmatrix}^T \qquad \textbf{Eq. A-24}$$

Eq. 3-67 can be rewritten as

$$\dot{x} = A_1 x + B_1 u, \qquad \textbf{Eq. A-25}$$

where u=v_{in}, and

$$A_1 = \begin{bmatrix} 0 & 0 & 0 & \dfrac{-1}{L_{1p}} \\ 0 & 0 & 0 & \dfrac{-1}{L_{2p}} \\ 0 & 0 & 0 & 0 \\ \dfrac{1}{C_{fp}} & \dfrac{1}{C_{fp}} & 0 & \dfrac{-1}{R_{LP}C_{fp}} \end{bmatrix} \qquad \textbf{Eq. A-26}$$

$$B_1 = \begin{bmatrix} 0 & \dfrac{1}{L_{2p}} & 0 & 0 \end{bmatrix}^T \qquad \textbf{Eq. A-27}$$

Similarly, for [DT, T], we have

$$\begin{aligned} L_m \frac{di_m}{dt} &= v_{in} - v_c \\ L_{1p} \frac{di_{1p}}{dt} &= v_c - v_{op} - v_{in} \\ L_{2p} \frac{di_{2p}}{dt} &= -v_{op} \\ C_c \frac{dv_c}{dt} &= i_m - i_{1p} = \frac{L_{2p}}{L_m} i_{2p} - \left(\frac{L_{1p}}{L_m} + 1 \right) i_{1p} \\ C_{fp} \frac{dv_{op}}{dt} &= i_{1p} + i_{2p} - \frac{v_{op}}{R_{LP}} \end{aligned} \qquad \textbf{Eq. A-28}$$

The fourth equation in Eq. A-28 has utilized Eq. A-22. Again, if we use only the four variables i_{1p}, i_{2p}, v_c, and v_o to form the state space equation, we will have

$$\dot{x} = A_2 x + B_2 u \qquad \textbf{Eq. A-29}$$

where

$$A_2 = \begin{bmatrix} 0 & 0 & \frac{1}{L_{1p}} & \frac{-1}{L_{1p}} \\ 0 & 0 & 0 & \frac{-1}{L_{2p}} \\ \frac{-(L_{1p}+L_m)}{C_c L_m} & \frac{-L_{2p}}{C_c L_m} & 0 & 0 \\ \frac{1}{C_{fp}} & \frac{1}{C_{fp}} & 0 & \frac{-1}{R_{LP} C_{fp}} \end{bmatrix} \quad \textbf{Eq. A-30}$$

and $$B_2 = \begin{bmatrix} \frac{-1}{L_{1p}} & 0 & 0 & 0 \end{bmatrix}^T \quad \textbf{Eq. A-31}$$

The state-space average technique will give

$$\dot{X} = AX + BU \quad \textbf{Eq. A-32}$$

$$A = dA_1 + d'A_2 = \begin{bmatrix} 0 & 0 & \frac{d'}{L_{1p}} & \frac{-1}{L_{1p}} \\ 0 & 0 & 0 & \frac{-1}{L_{2p}} \\ \frac{-d'(L_{1p}+L_m)}{C_c L_m} & \frac{d' L_{2p}}{C_c L_m} & 0 & 0 \\ \frac{1}{C_{fp}} & \frac{1}{C_{fp}} & 0 & \frac{-1}{R_{LP} C_{fp}} \end{bmatrix} \quad \textbf{Eq. A-33}$$

$$B = dB_1 + d'B_2 = \begin{bmatrix} \frac{-d'}{L_{1p}} & \frac{d}{L_{2p}} & 0 & 0 \end{bmatrix}^T \quad \textbf{Eq. A-34}$$

where d is the duty cycle, and d'=1-d.

For i_m, the average technique gives

$$L_m \frac{di_m}{dt} = v_{in} - d'v_c \quad \textbf{Eq. A-35}$$

Figure A-8shows the equivalent circuit for the average model described in Eqs. (A-32~35).

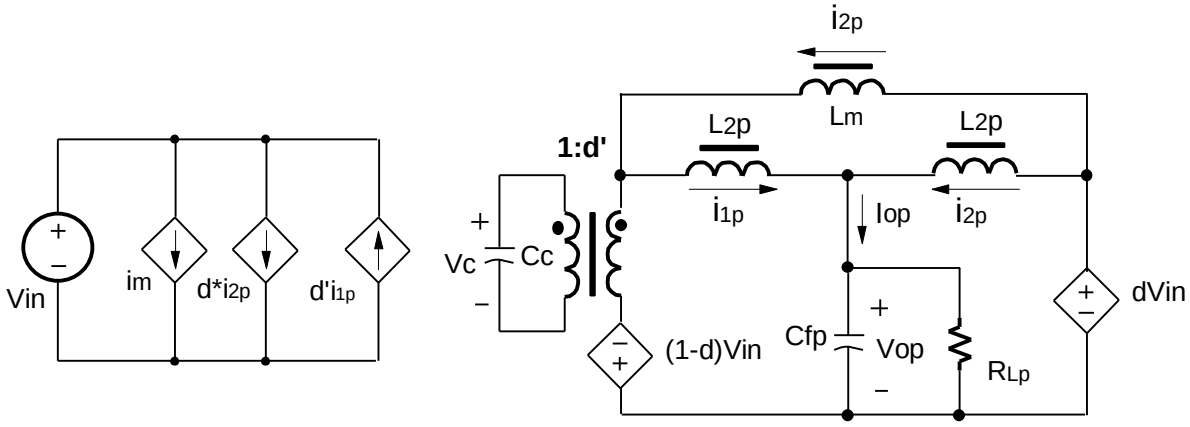

Figure A-8 Average circuit model for power stage

A.2.2. Transfer functions

By introducing the perturbations to the average model derived previously, we can derive the small signal model as follows:

$$\dot{\hat{X}} = A\hat{X} + B\hat{U} + P\hat{d} \qquad \textbf{Eq. A-36}$$

where

$$P = (A_1 - A_2)X_{dc} + (B_1 - B_2)U_{dc} \qquad \textbf{Eq. A-37}$$

$$X_{dc} = \begin{bmatrix} I_{1pdc} \\ I_{2pdc} \\ V_{cdc} \\ V_{indc} \end{bmatrix} = \begin{bmatrix} \dfrac{L_{2p}I_{op}}{L_{1p} + L_{2p} + L_m} \\ \dfrac{L_{1p} + L_m}{L_{1p} + L_{2p} + L_m} I_{op} \\ \dfrac{V_{indc}}{1 - D} \\ V_{indc} \end{bmatrix} \qquad \textbf{Eq. A-38}$$

Then the following transfer functions can be derived from the Laplace transform of Eq. A-36:

$$G_{Xd} = \left.\frac{\hat{X}}{\hat{d}}\right|_{\hat{U}=0} = (sI - A)^{-1}P \qquad \textbf{Eq. A-39}$$

$$G_{XU} = \left.\frac{\hat{X}}{\hat{U}}\right|_{\hat{d}=0} = (sI - A)^{-1} B \qquad \textbf{Eq. A-40}$$

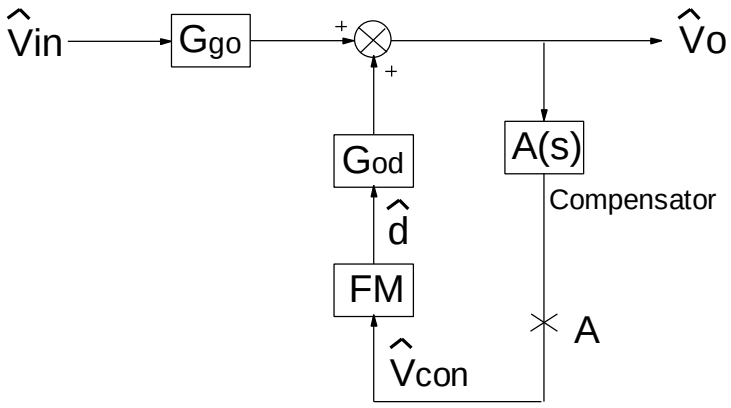

Figure A-9 Simplified block diagram of voltage mode control

Figure A-9 shows the simplified block diagram for the voltage mode control. All of the transfer functions defined in Figure A-9 can be solved from Eqs. A-39 and Eq. A-40. In the practical control loop design, Point A in Figure A-9 is usually broken to measure the Control to Output transfer function, which is represented by

$$G_{oc} = \frac{\hat{V}_o}{\hat{V}_{con}} = G_{od} \cdot FM \qquad \textbf{Eq. A-41}$$

where FM is the PWM modulation gain. G_{od} is expressed as follows:

Duty-cycle to output function G_{od}

$$G_{od} = \left.\frac{\hat{V}_o}{\hat{d}}\right|_{\hat{U}=0} = \frac{1 + s^2\left(C_c L_{1p} L_m - C_c L_{2p} L_m \frac{D}{D'}\right) \Big/ \left[D'^2\left(L_{1p} + L_{2p} + L_m\right)\right]}{\Delta(s)} \frac{V_{in}}{N}$$

Eq. A-42

where D is the steady state duty cycle, D'=1-D, and

$$\Delta(s) = 1 + s\frac{L_{2p}\left(L_{1p}+L_m\right)}{R_{LP}\left(L_{1p}+L_{2p}+L_m\right)} + s^2\left[\frac{L_{2p}\left(L_{1p}+L_m\right)C_{fp}}{L_{1p}+L_{2p}+L_m} + \frac{L_m\left(L_{1p}+L_{2p}\right)C_c}{\left(L_{1p}+L_{2p}+L_m\right)D'^2}\right] + s^3\frac{C_c L_{1p}L_{2p}L_m}{R_{LP}D'^2\left(L_{1p}+L_{2p}+L_m\right)} + s^4\frac{C_c L_{1p}L_{2p}L_m C_{fp}}{D'^2\left(L_{1p}+L_{2p}+L_m\right)}$$

Eq. A-43

The control-to-output function consists of two pairs of double–poles and two zeroes. When the duty cycle is smaller than the critical point, i.e.,

$$D < D_{crit} = \frac{L_{1p}}{L_{1p}+L_{2p}} = \frac{L_1}{L_2+L_1} = \frac{R_2}{R_1+R_2}, \qquad \textbf{Eq. A-44}$$

the transfer function contains a pair of complex zeroes,:

$$s_z = \pm j2pf_z$$
$$f_z = \frac{1-D}{2p\sqrt{\frac{C_c L_m\left|-L_{2p}\frac{D}{1-D}+L_{1p}\right|}{L_{1p}+L_{2p}+L_m}}} \qquad \textbf{Eq. A-45}$$

At complex zeroes, the phase will be boosted by 180 degree.

If D>Dcrit, the transfer function contains a pair of real zeroes:

$$s_z = \pm 2pf_z. \qquad \textbf{Eq. A-46}$$

Note that the phase at real zeroes will not be boosted. The difference between the real zeroes and complex zeroes is demonstrated in the plots of Figure A-10.

All of the poles are the functions of duty cycle, L1, L2, Lm, Cf, Cc, and RL. They can be solved from Eq. A-39~40. The close form expressions are too complicate. Pspice simulation of the average circuit model is still an easy way to locate the pole-zero positions.

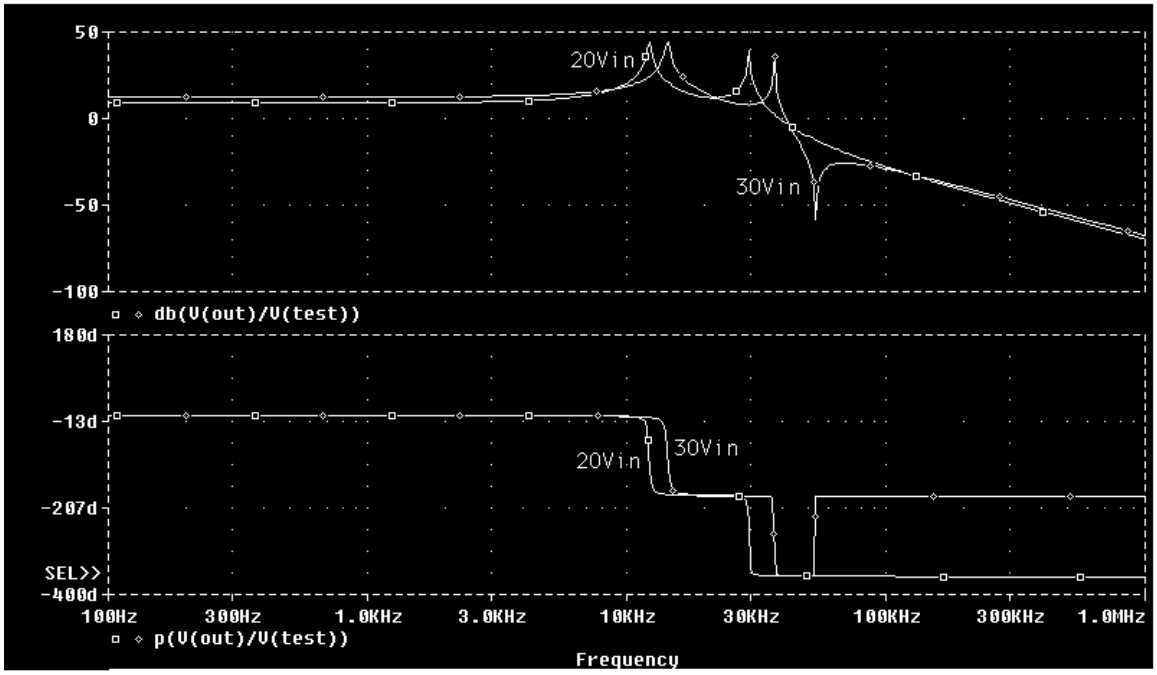

Figure A-10 Control-to-Output Function under Different Duty Cycle

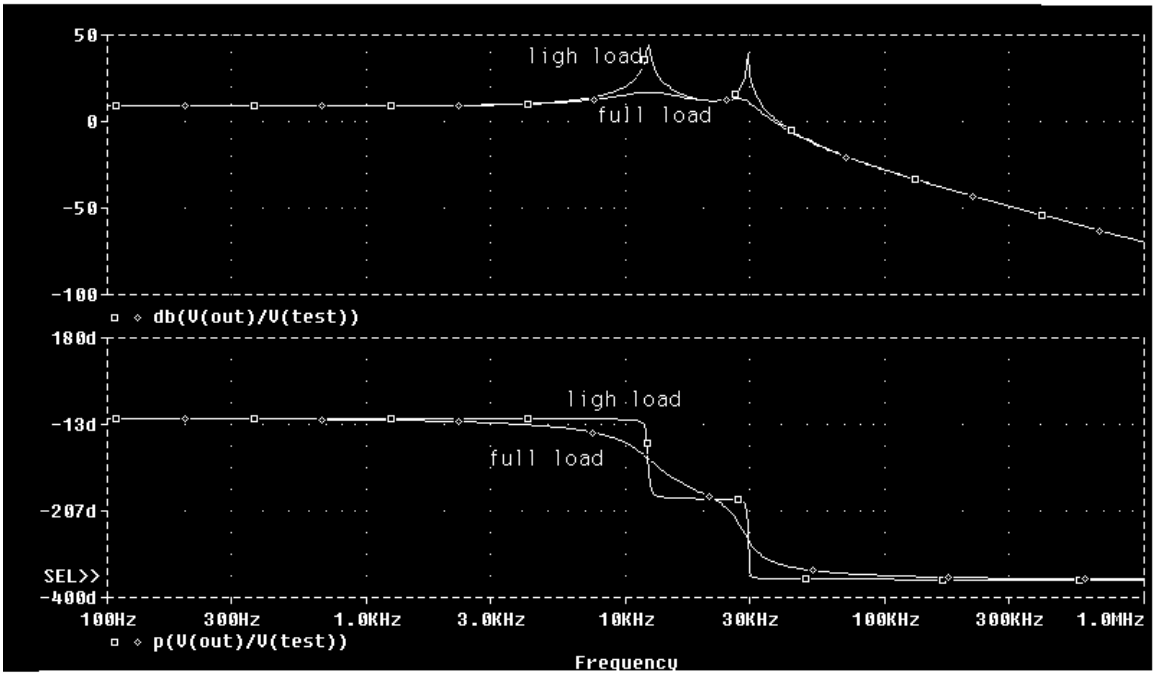

(a) Vin = 20 V

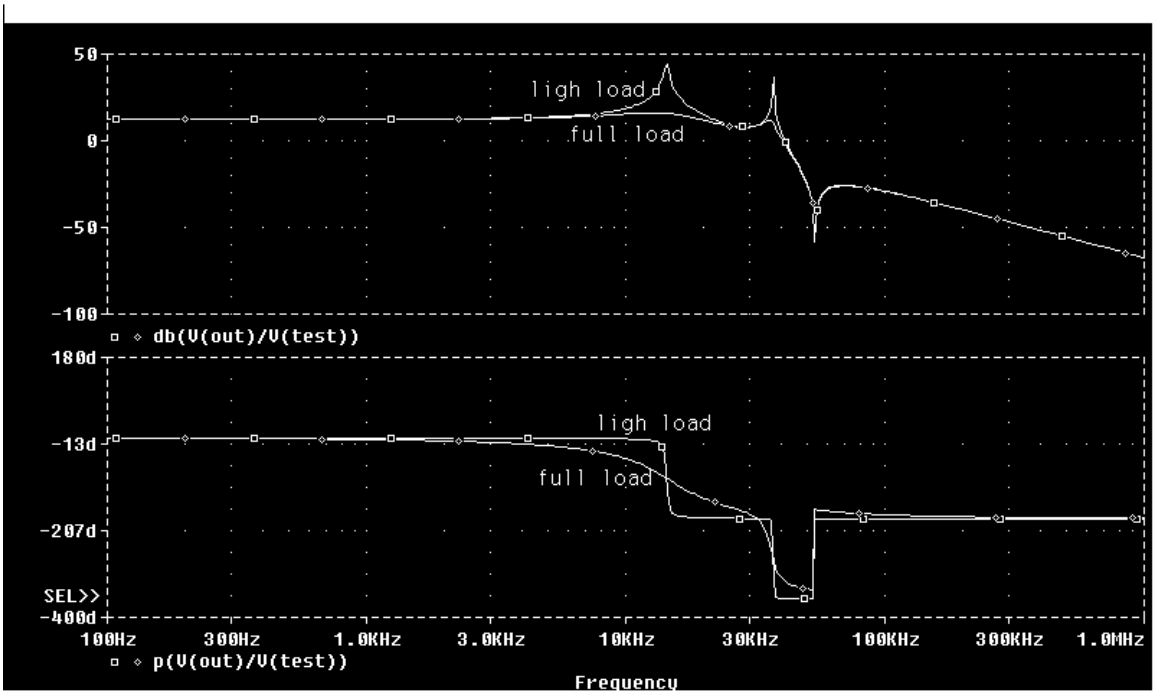

(b) Vin =30 V

Figure A-11 Control-to-Output Function under Different Load Condition

A.2.3. Current mode control

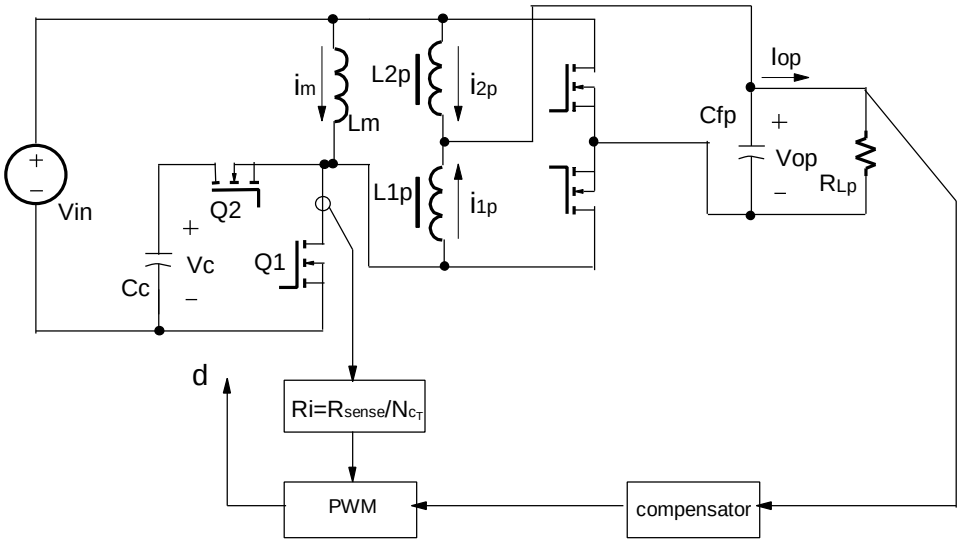

Figure A-12 Simplified Diagram of Power Stage with Current Mode Control

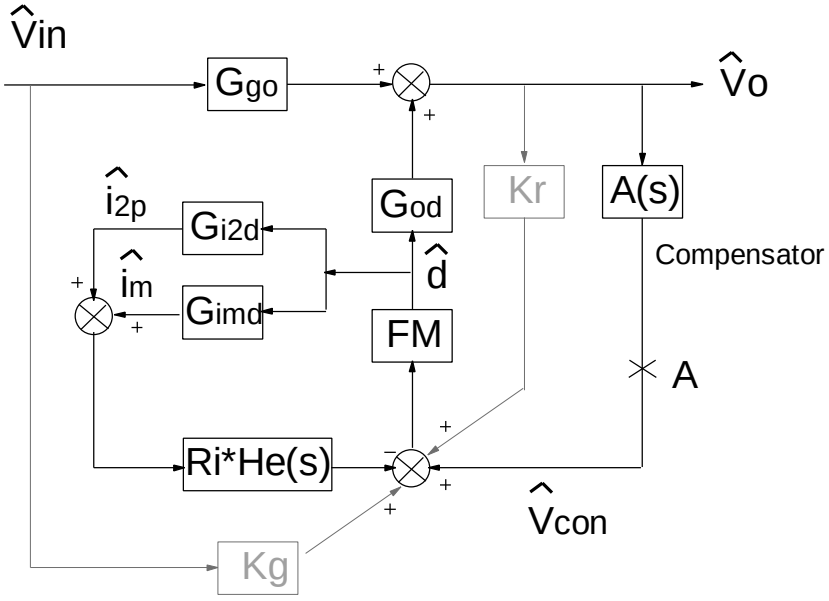

Figure A-13 Block diagram with Current loop

Figure A-12 shows the simplified diagram of power stage with current mode control. By employing the current mode control model provided in [D7], the block diagram of the complete system with current loop is shown in Figure A-13. The feedforward terms Kr

and Kg are usually very small, they are neglected in the following discussion. The sampling function [D7] He(s) is expressed as

$$He(s) \cong 1 + \frac{s}{Q_z \cdot w_n} + \frac{s^2}{w_n^2} \qquad \textbf{Eq. A-47}$$

where

$$w_n = pf_s$$
$$Q_z = \frac{-2}{p} \qquad \textbf{Eq. A-48}$$

and f_s is the switching frequency.

If point A in Figure A-13 is broken apart to measure the "control" to output function and loop gain, the control to output function with current mode control can be derived. However, the expression is too long and too complicate. The simulation of the average circuit model shown in Figure A-8 appears to be more suitable for generating the plots of the transfer functions.

Figure A-14 shows the plots of the control-to-output function with current mode control. The first pair of double-poles (the lowest frequency) is split due to the introduction of current mode control: one pole is pushed to a lower frequency, while the other pole migrates to a higher frequency. The second pair of poles is slightly affected. And the zeroes at low duty cycle remain unchanged.

Stability Condition Discussion:

For both voltage mode and current mode control, the light load and low line condition is the worst case for the control loop design.

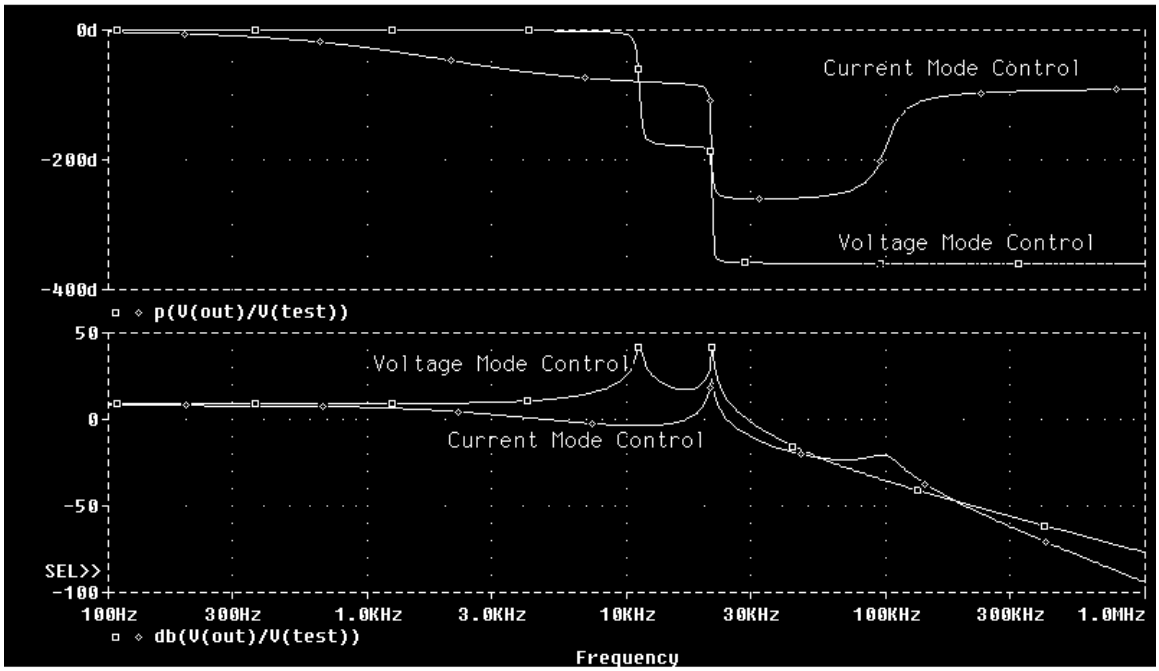

(a) $D>D_{crit}$

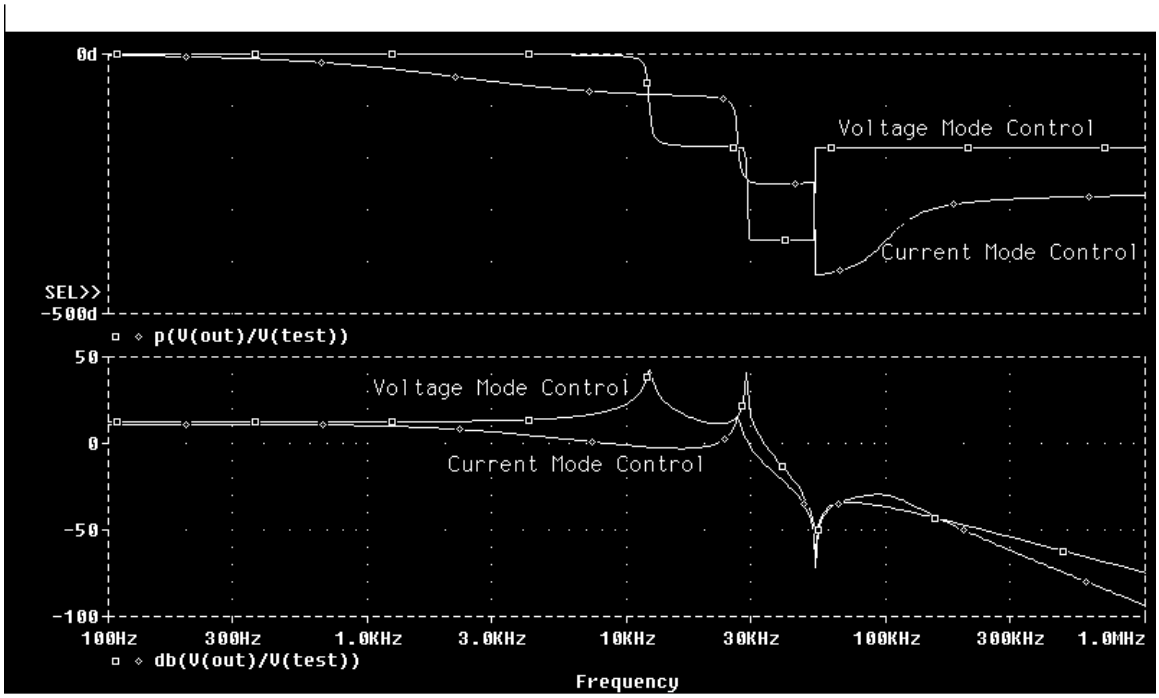

(b) $D<D_{crit}$

Figure A-14 Plots of control-to-output function with current loop (Ri=0.5 for current mode control)

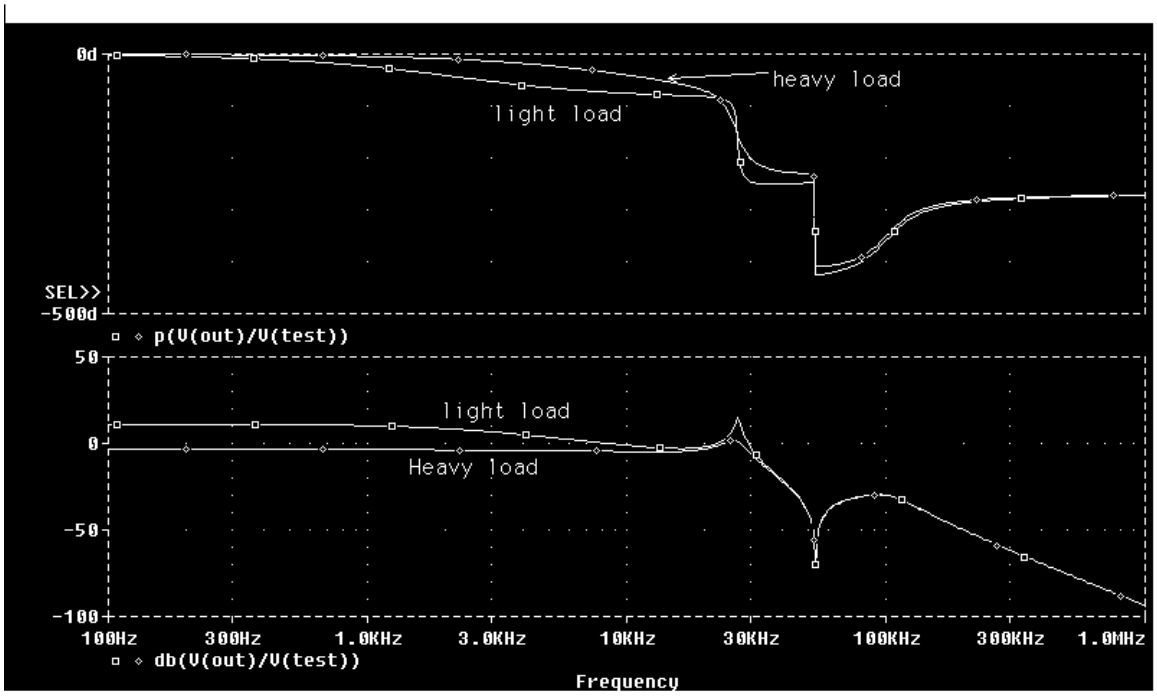

Figure A-15 Control-to-output function of current mode control under different load conditions (D<Dcrit)

A.3. Analysis of Soft-Switching Technique in Forward Improved Integrated Magnetic Circuits

In high power applications, large MOSFETs will be adopted for both Q1 and SRs (Q3,4). The turn-on loss in Q1 at high switching frequency may be excessively large because the effective capacitance across the drain to the source of Q1 is quite large. To analyze the mechanism for the soft-switching, the equivalent circuit of a FI^2M circuit is employed. To simplify the discussion, the leakage inductances of the windings are neglected.

Figure A-16 shows the turn-on procedures of Q1. It consists of two stages:

Vds1>Vin:

After Q2 turns off, the magnetizing inductance (Lm) current, along with the reflected L1 current, discharges Cp. The primary winding voltage gradually reduces to zero. If the magnitude of the magnetizing current is larger than the reflected L2 current, then the next stage continues. Otherwise, Q1 can be turned on with Vin applying on it.

Vds1<Vin:

The magnetizing current will supply the reflected L2 current and the discharging current for Cp. As the voltage on Cp is discharged to zero, the body diode of Q1 conducts. Q1 can then be turned on at zero voltage.

The delay time between Q2 turn-off and Q1 turn-on is estimated to be

$$t_N \approx \frac{C_p V_{in} D}{(1-D) I_{pN}} + \frac{C_p V_{in}}{\left| I_{mN} - I_{L2N} / N \right|} \qquad \textbf{Eq. A-49}$$

The condition for achieving ZVS is

$$I_{mN} > I_{L2N} / N \qquad \textbf{Eq. A-50}$$

where

$$I_{mN} \cong -I_{mdc} + \frac{\Delta I_m}{2}, \qquad \textbf{Eq. A-51}$$

$$I_{L1N} \cong I_{L1dc} + \frac{\Delta I_{L1}}{2}, \qquad \textbf{Eq. A-52}$$

$$I_{L2N} \cong I_{L2dc} - \frac{\Delta I_{L2}}{2}, \qquad \textbf{Eq. A-53}$$

$$I_{pN} \cong \left| I_{mN} - I_{L1N} \middle/ N \right| = \frac{\Delta I_{L1}}{2N} + \frac{\Delta I_m}{2} \qquad \textbf{Eq. A-54}$$

By substituting Eqs. A-51~54 into Eq. 3-50, and some simple calculations, the ZVS condition can be obtained as

$$\frac{\Delta I_m}{2} > \frac{I_o}{N} - \frac{\Delta I_{L2}}{2} \quad \text{or} \quad \frac{N}{L_m} > \frac{2 f_s I_o}{V_o} - \frac{1-D}{L_2} \qquad \textbf{Eq. A-55}$$

As seen from Eq. A-55, the light load and high line (small D) conditions are easier to achieve ZVS. Decreasing L2 or Lm can help extend ZVS range.

Q2 turns off, Vds1>Vin

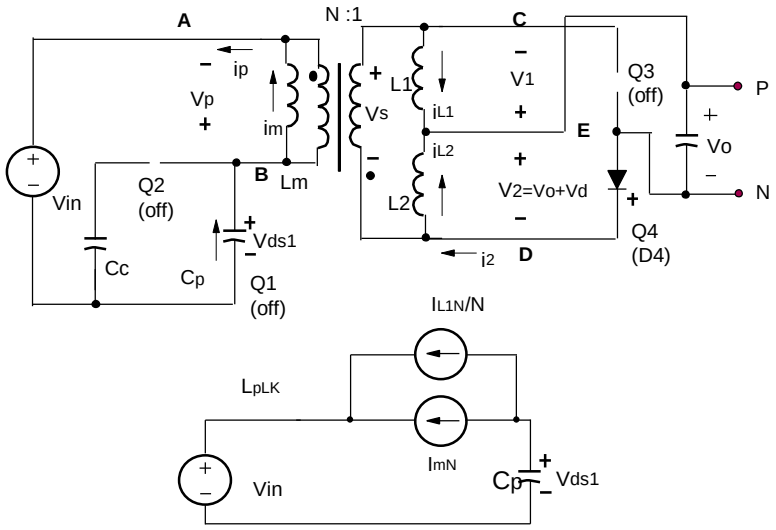

(a)

Q2 turns off, Vds1<=Vin

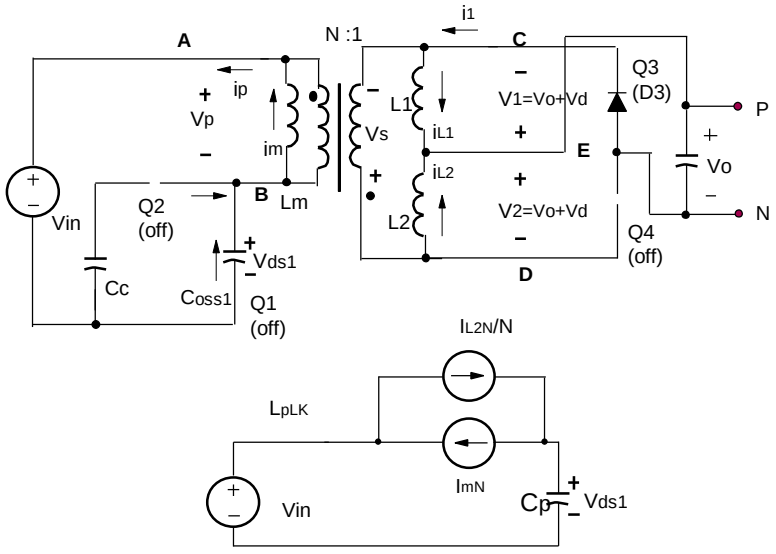

(b)

Figure A-16 Turn-on procedure of Q1

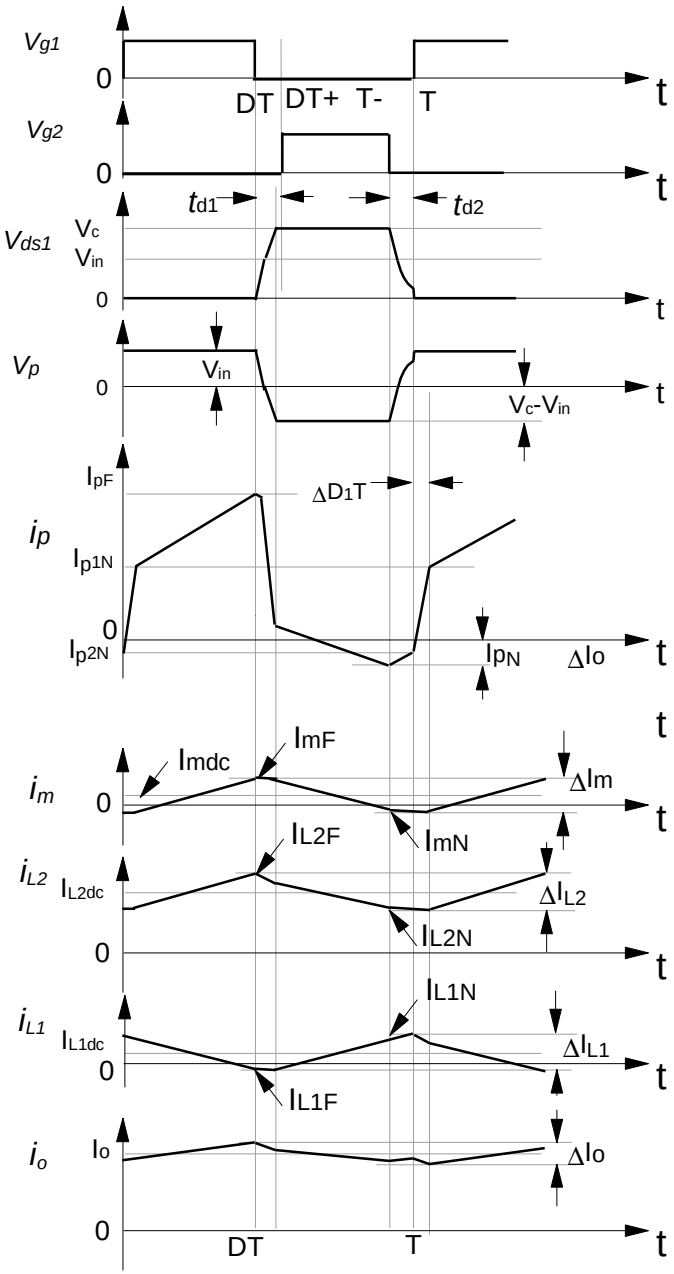

Figure A-17 Waveform in FI^{2}M considering switching transient

A.4. Equivalent electrical circuits for proposed integrated magnetic structure

The electrical circuit models are usually easy to understand than the magnetic structure. The methodology derived in [B5] is adopted for the derivation of the electrical equivalent circuit models. Figure A-18 defines the fluxes. Figure A-19 shows the derived results.

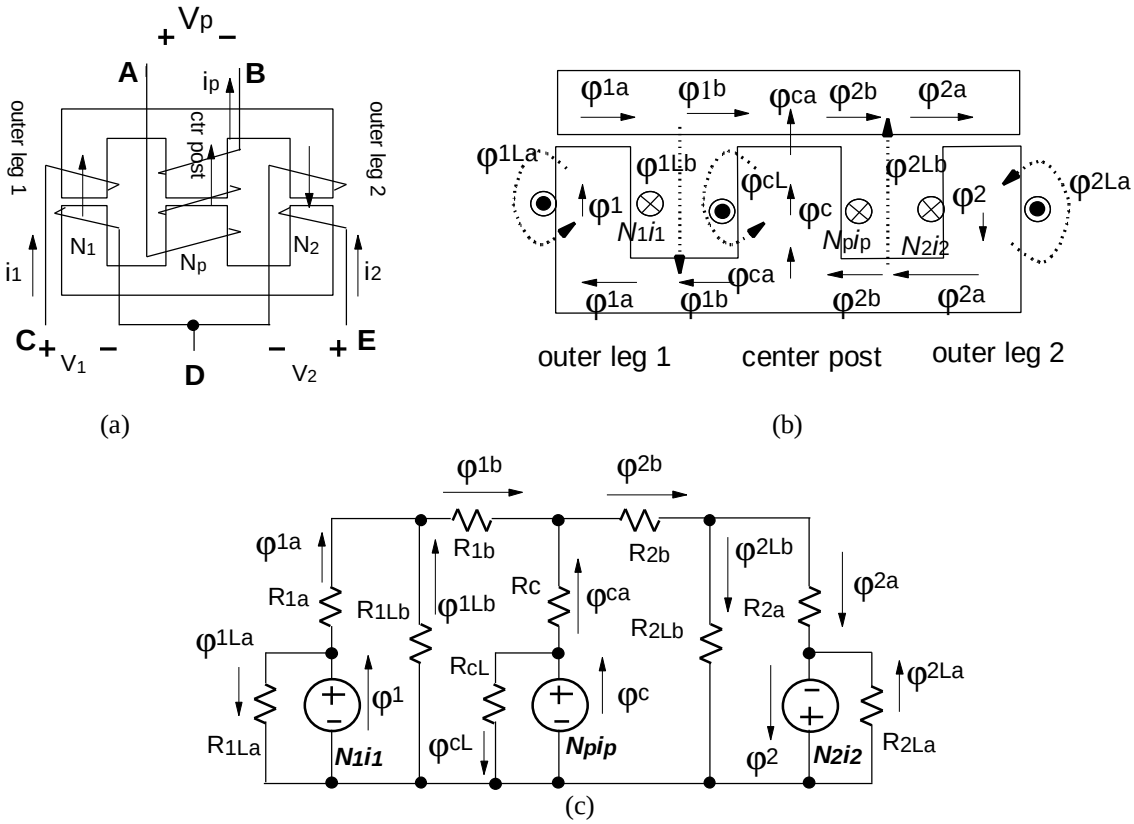

Figure A-18 Derivation of magnetic reluctance circuit for the proposed integrated magnetic structure: (a) proposed integrated magnetic structure, (b) definition of winding currents and fluxes, (c) magnetic reluctance circuit

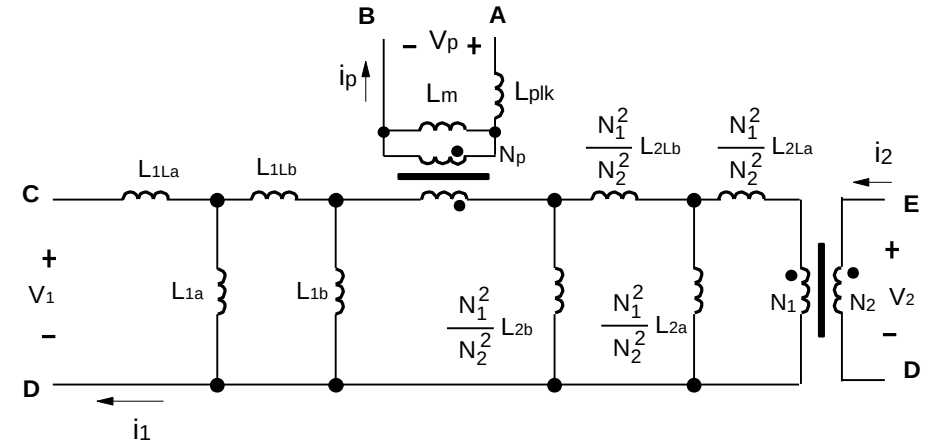

(a)

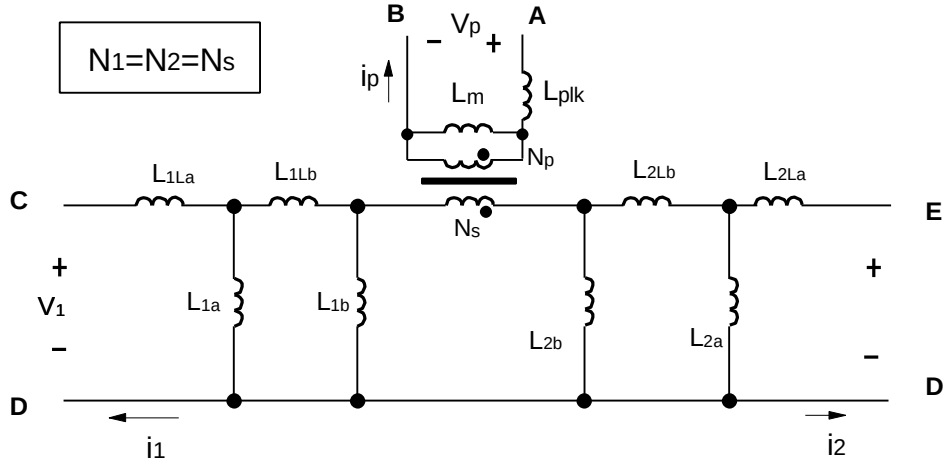

(b)

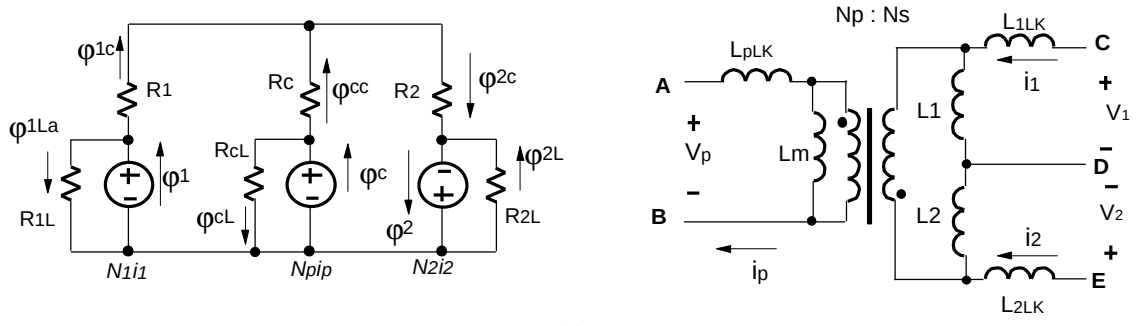

(c)

Figure A-19 Electrical circuit model of proposed IM structure: (a) complete electrical equivalent circuit model, (b) equivalent circuit when $N_1=N_2$, (c) magnetic reluctance circuit (left) and electrical equivalent circuit (right) when $N_1=N_2$ and j_{1Lb} and j_{2Lb} are neglected